Contents lists available at SciVerse ScienceDirect

Biochimica et Biophysica Acta

journal homepage: www.elsevier.com/locate/bbabio

An investigation into a cardiolipin acyl chain insertion site in cytochrome *c*

Badri S. Rajagopal [1], Gary G. Silkstone [1], Peter Nicholls, Michael T. Wilson, Jonathan A.R. Worrall *

School of Biological Sciences, University of Essex, Wivenhoe Park, Colchester, CO4 3SQ, UK

ARTICLE INFO

ABSTRACT

Mitochondrial cytochrome *c* associates with the phosphoplipid cardiolipin (CL) through a combination of electrostatic and hydrophobic interactions. The latter occurs by insertion into cytochrome *c* of an acyl chain, resulting in the dissociation of the axial Met-80 heme-iron ligand. The resulting five coordinate cytochrome *c*/CL complex has peroxidatic properties leading to peroxidation of CL and dissociation of the complex. These events are considered to be pre-apoptotic and culminate with release of cytochrome *c* from the mitochondria into the cytoplasm. Two distinct surface regions on cytochrome *c* have been suggested to mediate CL acyl chain insertion and this study has probed one of these regions. We have constructed a series of alanine mutants aimed at disrupting a surface cleft formed between residues 67–71 and 82–85. The physicochemical properties, peroxidase activity, CL binding, and kinetics of carbon monoxide (CO) binding to the ferrous cytochrome *c*/CL complex have been assessed for the individual mutants. Our findings reveal that the majority of mutants are capable of binding CL in the same apparent stoichiometry as the wild-type protein, with the extent to which the Met-80 ligand is bound in the ferrous cytochrome *c*/CL complex being mutant specific at neutral pH. Mutation of the species conserved Arg-91 residue, that anchors the cleft, results in the greatest changes to physicochemical properties of the protein leading to a change in the CL binding ratio required to effect structural changes and to the ligand-exchange properties of the ferrous cytochrome *c*/CL complex.

© 2012 Elsevier B.V. All rights reserved.

1. Introduction

In multicellular organisms, a regulated process of programmed cell death, commonly referred to as apoptosis, eliminates unwanted cells. This intracellular process is vital for development, homeostasis and immune defense and occurs through two main routes: the extrinsic pathway and intrinsic pathway [1]. The latter is also known as the mitochondrial pathway and is activated by stimuli that lead to the permeabilization of the outer mitochondrial membrane causing release of several pro-apoptotic proteins from the intermembrane space into the cytoplasm [2]. One of the proteins released is cytochrome *c* (cyt *c*), a small water-soluble heme protein best known for its role as a redox component of the mitochondrial electron transfer (ET) chain, where it shuttles electrons from the cytochrome bc_1 complex to cyt *c* oxidase [3]. Upon release from the mitochondrion, cyt *c* triggers apoptosis through a mechanism that involves interaction with Apaf-1, pro-caspase-9 and dATP/ATP to form the multi-component cellular assembly known as the apoptosome [4]. Thus

cyt *c* holds a pivotal position linking the redox chemistry driving oxidative phosphorylation with a process leading to programmed cell death, itself energy requiring. Factors giving rise to cyt *c* release from the mitochondrion have been a subject of much debate and are discussed extensively in the excellent review by Ow et al. [1].

Kagan and co-workers have elegantly shown that the interaction of cyt *c* with a phospholipid, diphosphatidylglycerol, commonly referred to as cardiolipin (CL), plays a key role in the release of pro-apoptotic factors from the mitochondrion, including cyt *c* itself [5]. CL is a unique phospholipid, found exclusively in the inner mitochondrial membrane, possessing a dimeric structure with four acyl groups and two negative charged bisphosphoglycerol head groups. A survey by Nicholls some three decades ago highlighted membrane interactions of cyt *c* and stimulated research interest into the nature of the reaction between cyt *c* and CL [6]. The preceding research, in many ways, has culminated in the discovery of a role for the cyt *c*/CL complex in triggering apoptosis. The complex formed between the positively charged ferric cyt *c* and CL causes the heme to become 5-coordinate (5C) and a mechanism involving a Compound I oxoferryl intermediate in the presence of peroxide has been proposed to result in the oxidation of CL [5,7–10]. A significant proportion of the ferrous cyt *c*/CL complex will also be present in mitochondria due to the presence of glutathione. The analysis of redox potential changes in the cyt *c*/CL complex has highlighted an alternative route to Compound I that is akin to cyt P450s and involves the ferrous cyt *c*/CL complex reacting with molecular oxygen and a further electron

from glutathione or ubiquinol [11]. Either way the resulting modified form of CL serves as a signal for downstream events, which lead to the permeabilization of the outer mitochondrial membrane and subsequent release of pro-apoptotic factors, most importantly cyt *c*, into the cytoplasm [5]. Once in the cytoplasm the ferric state of cyt *c* has been reported to regulate caspase activation [12]. These findings have led to the realization that cyt *c* has three roles in the cell: ET, promoting its own release from mitochondria via interaction with CL, and in assembling the apoptosome.

Structural details of the interaction between cyt *c* and CL at the atomic level are absent. Electrostatic interaction between the negatively charged bisphosphoglycerol head groups of CL and positively charged amino acids on the cyt *c* surface are perceived to be important, and it is now widely accepted that in addition to electrostatic effects a hydrophobic interaction plays a key role in triggering the peroxidatic activity of cyt *c* in the CL complex [8]. Kinnunen and co-workers proposed a model in which an acyl chain of a phospholipid could penetrate into the hydrophobic interior of cyt *c* [13–15]. Stewart et al. [16] proposed a similar interaction but also suggested that the acyl chain leads to disruption of the Met-80 ligand based upon the observation that the heme undergoes a spin-state change. Experimental support for this hypothesis came from a fluorescence spectroscopy study using a dibrominated lipid and Zn^{2+}-substituted cyt *c* [17], leading to a model named the extended lipid anchorage model. This model, although originally demonstrated for ferrous cyt *c*, is also likely to account for CL interacting with ferric cyt *c*, leading to disruption of the Met-80 heme-iron ligand and releasing the peroxidatic potential of the heme [5,7–9,18]. The presence of a double bond(s) in the acyl chains of CL was suggested to be critical for initiating the peroxidase activity of cyt *c* in the complex [5,7]. However, a recent study has indicated that the presence of a double bond (or bonds) in the fatty acyl chain is not essential for the induction of this peroxidase activity [19], which is probably a consequence of the intercalation of an acyl chain into the hydrophobic interior causing partial unfolding and release of the Met-80 ligand [20].

The entry port for insertion of an acyl chain is currently a matter of speculation. Suggestions for insertion sites involve surface openings leading to hydrophobic channels that position the acyl chain in close proximity to the Met-80 ligand. At present two separate regions on cyt *c* have been proposed to be entry sites for an acyl chain of CL (see Fig. 1A). One of these has been implicated from studies with ferrous yeast cyt *c*, whereby changes in binding strength of phospholipid liposomes were found to occur through alteration of a specific area of electrostatic surface potential of cyt *c* [16,21]. The location of the charges on the cyt *c* surface led the authors to suggest that a nearby region consisting of two parallel polypeptide strands incorporating

amino acids 67–71 and 82–85 formed a cleft for acyl chain insertion (Fig. 1B) [16,21]. Insertion through the cleft leads to a hydrophobic channel that lies to one side of the M80 heme-iron ligand and is proposed to aid in stabilizing the association (Fig. 1C) [16,21]. The cleft is 'zipped' together by a number of polar side-chain:backbone or backbone:backbone interactions. At the top of the cleft is the invariant R91, which through its guanidinyl group participates in a number of strong hydrogen bond interactions, including one with the side-chain hydroxyl group of S65 (Fig. 1B). Another invariant residue, N70, hydrogen bonds to the backbone carbonyl of F82 and the backbone carbonyl of L68 is hydrogen bonded to the backbone amide of G84 (Fig. 1B). K72 and K73 lie at the bottom of the cleft and have been proposed to facilitate an electrostatic interaction with the bisphosphoglycerol head group, stabilizing the complex, and enabling the acyl chain to slide through the crevice and into the hydrophobic channel [21]. In addition to K72 and K73, the nearby residues K87 and K86 have been reported to be part of the binding surface for anionic phospholipid containing bilayers [22,23]. Other studies using the ferric protein have reported a two-state transition for the binding process of CL to cyt *c* [24,25]. This involves the binding to a high affinity electrostatic site (called site A), followed by binding to a low affinity hydrophobic site (called site C) [25]. The A-site is suggested to be in the region of K72 and K73 and the C-site close to the invariant N52 where a putative hydrophobic channel that can accommodate an acyl chain has also been identified [24]. Evidence for the involvement of the C-site has been obtained upon mutating N52 to an Ile, leading to the loss of the second binding transition [24]. This has been interpreted to mean that the second site for the insertion of an acyl chain from a single CL molecule is centered around N52 with the first site for acyl chain insertion being at the proposed cleft (residues 67–71 and 82–85) identified from studies with the ferrous protein [21,24].

We have previously studied the ferrous cyt *c*/CL complex in the presence of the cell signaling/regulator molecule CO [18]. Under physiological conditions CO cannot bind to ferrous cyt *c*; however, upon formation of the ferrous cyt *c*/CL complex facile binding of CO can occur with an escape probability on photolysis in the region of 80% [18]. The binding of CL and subsequent protein rearrangement therefore creates an efficient gas-exchange pathway in the cyt *c* molecule as found in gas binding hemoproteins such as myoglobin [18]. The nanomolar affinity for CO and the subsequent inhibition of peroxidase activity in the complex makes a role for CO in pre-apoptotic events in the mitochondrion a possibility [18]. An advantage of the ferrous cyt *c*/CL complex being able to bind CO is that it provides a spectroscopic handle to probe dynamic ligand binding events in the protein–lipid complex. The CO–heme bond can be photolyzed with a high apparent quantum yield and CO rebinding followed
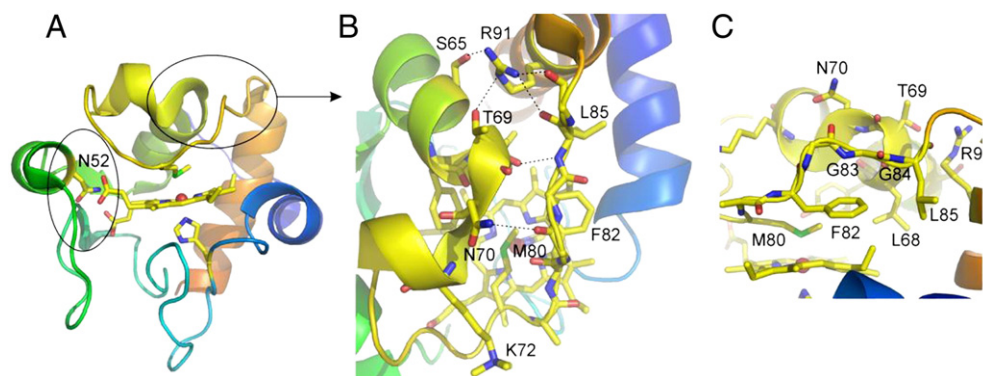

Fig. 1. The X-ray crystal structure of yeast cyt *c* (pdb entry 1YCC). (A) The circles indicate two regions of the protein proposed to interact with CL via the extended lipid anchorage model. The heme and axial ligands are shown in sticks along with the residue Asn52 (see text for details). (B) A detailed view of the amino acids that form a cleft to accommodate the insertion of one acyl chain of CL. The cleft is held together by a number of hydrogen bond interactions, indicated by dashed lines. (C) A view of the putative hydrophobic channel lying beneath the cleft that serves to stabilize the inserted acyl-chain of CL. A number of amino acids are labeled to orientate the view for comparison with that in B.

spectroscopically [26,27]. This allows for the interplay between intrinsic and external ligands to be probed and the dynamics of the heme environment in the CL complex to be explored.

In the present study, we have set out to explore further the cleft region formed by amino acids 67–71 and 82–85 proposed by Kalanxhi and Wallace [21] to be a site of acyl chain insertion. We have constructed a series of site-directed mutants that have been designed to interrupt a number of polar interactions that are perceived to be important for the structural integrity of the cleft. The effect of each introduced mutation on the spectroscopic properties, heme midpoint redox potential (E_m) and thermodynamic stability has also been characterized with respect to the wild-type (WT) protein. The effect the mutations have upon binding CL to the ferric and ferrous protein have been assessed by monitoring peroxidase activity, CO binding and laser flash photolysis kinetics. We find that the conserved R91 has the greatest influence on the stability of the cleft leading to facile CO binding and increased peroxidase activity.

2. Materials and methods

2.1. Site-directed mutagenesis and over-expression of yeast cyt c and mutants

The *Escherichia coli* plasmid, pUC18 (Amp[r]), harboring the genes for yeast cyt *c* and yeast heme lyase [28], was used as a template to introduce nucleotide changes into the cyt *c* gene using a method based on Stratagene's Quikchange mutagenesis procedure [29]. The yeast cyt *c* gene used as a template for the mutagenesis encodes for a protein with two mutations (T-5A/C102T) and is referred to as wild-type (WT). The forward and reverse primers used to introduce the respective mutations together with the PCR conditions are reported in Table S1 (Supporting information). All clones were sequenced to corroborate that the intended mutations were successfully introduced. Over-expression of the WT protein and mutants was carried out in GM119 or JM109 *E. coli* cells. Growth conditions and purification for the WT and all mutants were essentially the same as previously reported [28]. Purified protein samples for ESI-MS analysis were first exchanged into 1 M ammonium acetate and then diluted 1:20 with 50% methanol and 1% formic acid. Masses of the WT and mutants were determined using a Micromass Quattro Ultima triple quadrupole mass spectrometer operating in positive ion detection mode.

2.2. UV–visible and circular dichroism spectroscopy

UV–Vis spectra of WT and mutant proteins were acquired between 800 and 250 nm using a Varian Cary 5E or Cary 50 spectrophotometer (Palo Alto, USA) fitted with a thermostatted cell holder controlled by a Peltier system. Protein concentrations were determined by using either the molar extinction coefficient $\varepsilon = 27.5$ mM^{-1} cm^{-1} at 550 nm for ferrous cyt *c* or $\varepsilon = 106$ mM^{-1} cm^{-1} at 409 nm for ferric cyt *c*. The ferric or ferrous protein was prepared by the addition of excess K$_3$[Fe(CN)$_6$] or ascorbic acid, respectively, followed by removal using a PD10 column (GE Healthcare). Circular Dichroism (CD) measurements were carried out using an Applied Photophysics Chirascan CD spectrophotometer (Leatherhead, UK) with a thermostatted cell holder controlled by a Peltier system. Far-UV CD spectra at 20 °C for WT and mutants were acquired in the range 280–190 nm.

2.3. Chemical and thermal denaturation

Ultrapure guanidine hydrochloride (GuHCl) was purchased from Fluka (>99%) and a stock solution of 6 M prepared by dissolving solid GuHCl in 10 mM potassium phosphate, 50 mM potassium fluoride pH 7.0, and filtered through a 0.22-μm filter (Millipore) before use. Proteins were exchanged into 10 mM potassium phosphate,

50 mM potassium fluoride pH 7.0 using a PD-10 column (GE Healthcare). Protein concentrations were ~20 μM for both thermal and chemical denaturation experiments. Changes in the molar ellipticity at 222 nm (θ_{222nm}) were monitored for chemical and thermal denaturation studies. The 6 M stock solution of GuHCl was titrated into a protein sample to give the final desired [GuHCl] with mixing facilitated by a magnetic stirrer. Thermal denaturation was monitored between 0 and 96 °C with changes in θ_{222nm} monitored at 1 °C intervals. The sampling time for each data point at the desired [GuHCl] or temperature was 12 s. Both the chemical and thermal denaturation were deemed to be reversible based upon >95% return to the starting helicity upon diluting out the GuHCl or cooling to 20 °C.

Unfolding data for chemical denaturation were fitted using an equation for two-state unfolding with the assumption of linear baselines for native and denatured proteins according to the method of Santoro and Bolen [30]

$$observable = \frac{(\alpha_N + \beta_N[GuHCl]) + (\alpha_D + \beta_D[GuHCl])\exp\left(\frac{-\Delta G_{D-N}^{H_2O} + m[GuHCl]}{RT}\right)}{1 + \exp\left(\frac{-\Delta G_{D-N}^{H_2O} + m[GuHCl]}{RT}\right)}$$

(1)

α_N and α_D correspond to the baseline values of the native and denatured protein at 0 M GuHCl, respectively, and β_N and β_D to their respective dependence on [GuHCl], i.e., the slope. $\Delta G_{D-N}^{H_2O}$ is the free energy of denaturation in water and m represents the dependence of the free energy of denaturation on [GuHCl]. The fraction denatured (F_D) at any given [GuHCl] was calculated from Eq. (2).

$$F_D = \frac{\theta_{222nm} - (\alpha_N + \beta_N[GuHCl])}{(\alpha_D + \beta_D[GuHCl]) - (\alpha_N + \beta_N[GuHCl])}$$

(2)

For thermal denaturation the data were fitted to the modified Gibbs-Helmholtz Eq. (3)

$$\Delta G_{D-N} = \Delta H_m\left(1 - \frac{T}{T_m}\right) - \Delta C_p\left[(T - T_m) + T\ln\left(\frac{T}{T_m}\right)\right]$$

(3)

where ΔG_{D-N} is the free energy change for protein denaturation as a function of temperature, ΔH_m is the enthalpy of denaturation, T_m is the temperature at which half of the protein is denatured and ΔC_p is the difference in heat capacity between the denatured and native states. For a monomeric system at the T_m $\Delta G_{D-N} = 0$ and hence $\Delta H = T\Delta S$ and the entropic component can be eliminated.

2.4. Alkaline transition measurements

The pH dependence of the 695 nm band in the red region of the cyt *c* spectrum was measured using a tricomponent buffer consisting of 10 mM CAPS/Tris/sodium phosphate at 25 °C with a small aliquot of K$_3$[Fe(CN)$_6$] present to maintain an oxidizing environment. Protein concentrations used were 100 μM. The pH was adjusted by microliter aliquots of 2 M NaOH. After each addition of NaOH the pH of the sample was measured and an absorbance reading at 695 nm was recorded. Data were fitted to a one-proton ionization equilibrium equation to yield an apparent pK_a.

2.5. Redox titrations

The midpoint redox potential (E_m) was analyzed spectrophotometrically by the equilibration method using N,N,N',N'-tetramethyl-*p*-phenylenediamine (TMPD, $E_m = +240$ mV) as a reference compound, which has an absorption band at 610 nm in its oxidized state. A 2.7 ml solution consisting of cyt *c* (5 μM), TMPD (10 μM) and ascorbate (10 μM) in 20 mM Hepes buffer (pH 7.4) was placed in a cuvette and absorbances of fully reduced cyt *c* (A$_{550}$–A$_{540}$) and

TMPD (A_{610}) were measured. This mixture was then sequentially oxidized by 1 μl additions of 5 and 10 mM $K_3[Fe(CN)_6]$ and absorbance values were acquired at each step. After consistent readings were recorded, an excess of $K_3[Fe(CN)_6]$ was added to fully oxidize both cyt c and TMPD. For each step, ratios of oxidized and reduced forms of cyt c and TMPD were calculated and these were plotted as log($TMPD_{OX}$/$TMPD_{RED}$) versus log(cyt c_{OX}/cyt c_{RED}), yielding a linear graph with a slope of 1 and a y-axis intercept of a where a*59.2 mV is equal to E_mTMPD – $E_m$cyt c according to the Nernst equation.

2.6. Peroxidase assays

Peroxidase activity of the ferric WT yeast cyt c and mutants in the presence and absence of CL was assayed using H_2O_2 and guaiacol (O-methoxyphenol; Sigma). The oxidation of guaiacol was monitored using a Hewlett-Packard 8453 diode-array spectrophotometer scanning between 700 and 350 nm and thermostatted at 25 °C. The reaction was initiated by the addition of 1 mM H_2O_2 to a series of cuvettes containing 5 μM cyt c and 0.6 mM guaiacol in a volume of 2.7 ml in 20 mM HEPES pH 7.4. Traces obtained from plotting the maximal rate of change in absorbance at the wavelength pair 470–600 nm versus [cyt c] were fit to a zero-order rate equation to obtain a rate in AU/s. Note that the maximal rate in the absence of CL is achieved only after a short lag phase (Fig. 3 Results). The rate of cyt c turnover as a peroxidase is reported in $μM\ s^{-1}$ obtained by dividing AU/s by the product concentration of oxidized guaiacol using 5.57 $mM^{-1}\ cm^{-1}$ as the guaiacol extinction coefficient at pH 7 [31]. These rates are proportional to k*[H_2O_2]*[cyt c^{3+}] and a second order rate constant can be derived by dividing the rate by the product of peroxide and cyt c concentration.

2.7. Cardiolipin and CO binding

Stock solutions of CL (sodium salt from Bovine heart; Sigma) were prepared in ethanol under a N_2 environment to avoid oxidation. The final concentration of ethanol in protein samples was kept to a minimum (~2%, never exceeding 5%) so as to avoid protein modification [18]. Stock CL was titrated in microliter aliquots to ferric protein samples (5 and 10 μM) followed by the formation of the CL-bound ferrous protein by the addition of a few grains of sodium dithionite under anaerobic conditions in the presence of nanomolar catalase to prevent bleaching of the heme by peroxide generated through reaction of dithionite with any remaining oxygen. The CO-bound form was subsequently formed by equilibration of the ferrous cyt c–CL complex with 1 atm CO. Steady-state spectra of the individual steps were recorded using a Cary 5E spectrophotometer thermostatted at 22 °C.

2.8. Kinetics of CO binding

Microsecond laser flash photolysis measurements were carried out on an Applied Photophysics (LKS.60) instrument at 22 °C and stopped flow measurements were carried out using an Applied Photophysics SX-20 instrument. Protein concentrations ranged between 3 and 7 μM. CL-bound ferric cyt c samples were prepared in the presence of 30-fold molar excess of CL followed by reduction to the ferrous form as described. Stock CO solutions were prepared by equilibration of de-gassed buffer held within a tonometer with pure CO at 20 °C (~1 mM in CO). The concentration of each stock CO solution was determined by titration against known concentrations of deoxymyoglobin (Horse heart; Sigma). Experiments were conducted under pseudo-first-order conditions with concentrations of CO ranging from 13 to 195 μM. Second-order rate constants were determined from the slopes of plots of observed pseudo-first-order rate constants versus CO concentration. For laser flash photolysis, the time resolved spectra were constructed over a spectral range of 375–450 nm by splining the kinetic data at 5-nm intervals. Thus, each experiment required 16 individual photolysis events at every 5 nm from 375 to 450 nm and which on assembly yielded kinetic data. For stopped-flow, the time resolved spectra were generated similarly to the flash method described (data not shown) by accumulating kinetic traces using photomultiplier detection at 3-nm intervals throughout the wavelength range explored and the whole data set was used to construct the time resolved spectra. Thus each experiment required 26 individual "shots," which on assembly yielded kinetic data points at 25-μs intervals (for the fastest time courses) and at 3-nm intervals on the wavelength scale.

3. Results

3.1. Construction and characterization of the cleft variants of yeast cyt c

To test whether the cleft formed between two parallel polypeptide strands 67–71 and 82–85 in cyt c is sensitive to CL binding and activity of the heme towards small molecules such as H_2O_2 and CO, alanine mutations of the side-chain residues, R91, T69, N70 and S65 were prepared. T69 was also substituted with a glutamate, which is found in horse heart and human cyt c. A K72A variant was also prepared. In native yeast cyt c K72 is trimethylated [32] but when over-expressed in $E.\ coli$ this modification does not occur [28]. This leads to K72 having a greater propensity than either K73 or K79 to deprotonate and replace Met-80 as the axial heme ligand at alkaline pH [33]. The K72A variant has therefore been reported to be a good mimic of the native trimethylated state in that displacement of Met-80 heme-iron ligand at alkaline pH does not affect the native alkaline conformers involving K73 and K79 [33]. All mutants were over-expressed in $E.\ coli$ and confirmation of the respected substitutions was obtained by denaturing ESI–mass spectrometry (Table 1). The UV–visible spectra were indistinguishable from that of the WT protein (data not shown) and in all cases the far-UV CD spectrum exhibited two negative minima at 208 and 222 nm, consistent with a fully folded protein dominated by an α-helical structure (Fig. 2A). The $θ_{222/208}$ nm ratio for the WT protein is 1.1 and for the cleft variants it ranged between 1.0 and 1.2, indicating that the variants do not significantly perturb global secondary structure. Far-UV CD spectroscopy was used to monitor global protein stability of the WT and mutant proteins either in the presence of increasing concentrations of GuHCl or by heating. Typical unfolding profiles are shown in Fig. 2B and C, along with the data fits, to yield thermodynamic unfolding parameters from the GuHCl data and T_m values from thermal denaturation data (Table 1). With the exception of the R91A variant the introduction of Ala residues at the chosen positions in the cleft have relatively minor effects on global stability (Table 1). For the R91A variant, however, significant changes are observed with a $\Delta\Delta G_{D-N}^{H_2O}$ of 2.5 kcal mol^{-1} and a ΔT_m of 6.4 °C, indicative of a significant destabilization of the ferric protein upon removal of the conserved Arg residue (Table 1).

The 695-nm band in the visible spectrum of ferric cyt c is bleached upon increasing the alkalinity of the solution, which represents a deprotonation event in which the Met ligand is dissociated [34,35]. The pK_{695} value of this transition has proven to be a good indicator of the relative stability of the Fe–S(Met) bond in the ferric protein and can therefore be considered a marker for local stability [36]. A typical example of a pH versus absorbance transition of the 695 nm band is given in Fig. 2D, and pK_{695} values for WT and all variants are reported in Table 1. In contrast to the global stability measurements significant variations in pK_{695} values are observed amongst the cleft variants. The R91A variant has a low pK_{695} value suggesting a less stable Fe–S(Met) interaction and a similar interpretation can be made for the S65A and N70A cleft variants (Fig. 2D and Table 1). The pK_{695} value of the K72A variant increases slightly relative to that of the WT protein (Table 1). This is not unexpected considering that K72 has a high propensity to replace the Met-80 ligand at alkaline

Table 1
Summary of physicochemical properties of yeast ferric cyt c and cleft mutants. Experimental conditions and fitting procedures are described in Materials and Methods.

Protein	Mass[a]	$\Delta G_{D-N}^{H_2O\,a,b}$	$m^{a,b}$	$C_m^{a,b}$	$T_m^{a,b}$	pK_{695}^{b}	$E_m^{a,c}$
WT	12634.8 ± 0.29 (12635.2)[d]	6.9 (0.5)	4.6 (0.3)	1.5 (0.1)	62.7 (2)	8.5 (0.1)	+ 247 (4)
S65A	12618.8 ± 0.46 (12619.2)[d]	6.1 (0.5)	4.3 (0.4)	1.4 (0.1)	61.8 (3)	7.9 (0.1)	+ 241 (3)
T69A	12604.1 ± 0.82 (12605.2)[d]	6.5 (0.4)	4.1 (0.4)	1.6 (0.1)	65.1 (2)	8.2 (0.1)	+ 242 (5)
T69E	12662.8 ± 0.52 (12663.2)[d]	7.1 (0.6)	4.9 (0.3)	1.5 (0.1)	63.1 (4)	8.3 (0.1)	+ 248 (3)
N70A	12591.6 ± 0.35 (12592.2)[d]	6.2 (0.5)	4.6 (0.3)	1.4 (0.1)	60.7 (2)	8.0 (0.1)	+ 243 (6)
K72A	12578.5 ± 0.55 (12578.1)[d]	7.1 (0.3)	4.6 (0.5)	1.6 (0.1)	63.7 (2)	8.8 (0.1)	+ 245 (2)
R91A	12550.8 ± 0.31 (12550.1)[d]	4.4 (0.4)	4.1 (0.4)	1.1 (0.1)	56.3 (2)	7.2 (0.1)	+ 217 (4)

[a] Da; $\Delta G_{D-N}^{H_2O}$ kcal mol^{-1}; m kcal mol^{-1} M^{-1}; C_m M; T_m °C; E_m mV vs. NHE.
[b] Values reported are an average of three measurements and numbers in parenthesis indicate the standard deviation.
[c] Errors reported for the E_m are the standard deviation from duplicate data sets.
[d] Predicted mass of holo-protein.

pH and is consistent with elevated pK_a values previously reported for the K72A mutant [33].

3.2. Redox potential of the cleft variants

The E_m values for the cleft variants were determined by an equilibration method using TMPD as the reference compound and ferricyanide as the redox potential modulator (Fig. 3A). The ionic strength of the solution can strongly influence the E_m of cyt c and we estimate our solution (20 mM HEPES pH 7.4) to have an ionic strength of approximately 8 mM. At this ionic strength and at a pH of 7.4 horse heart cyt c has a E_m of + 255 mV [31]. The E_m of TMPD under our

conditions was therefore determined using this value. In Table 1 the E_m values for the variants are reported. With the exception of the R91A variant, where a 30 mV decrease in E_m is observed, the introduced substitutions in the cleft region have only minor effects on the E_m.

3.3. Peroxidase activity of the cleft variants in the absence and presence of CL

Peroxidase activity for the ferric WT cyt c and the cleft variants was measured by monitoring guaiacol oxidation by H_2O_2. Fig. 3B shows some characteristic time courses for this process under our
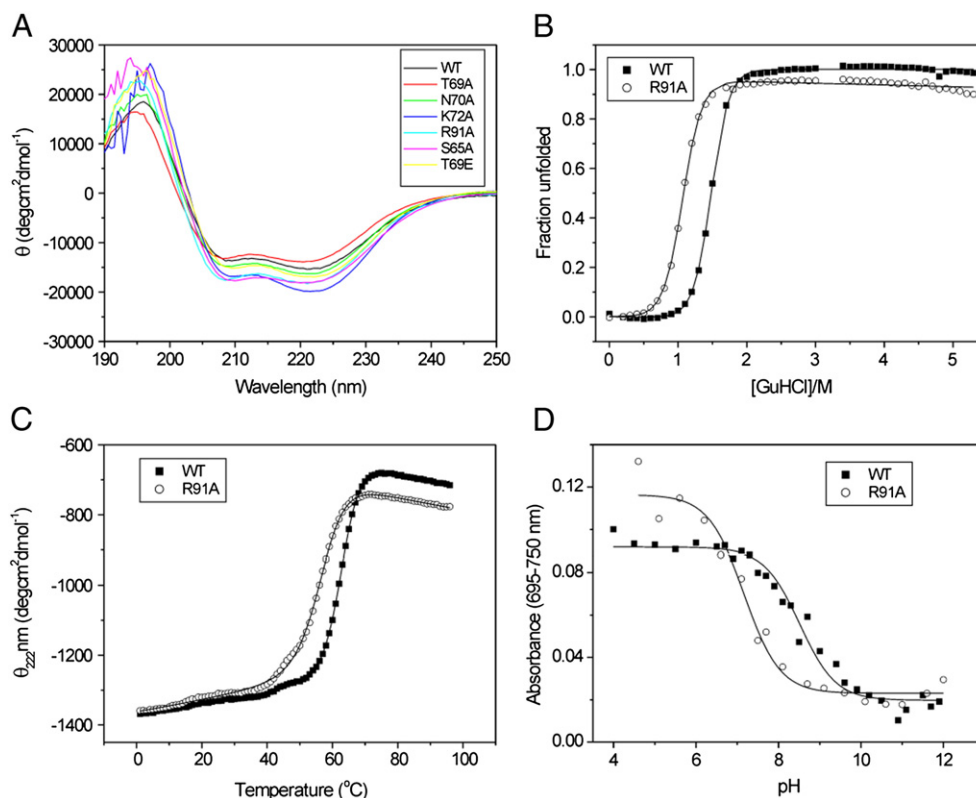

Fig. 2. (A) Far-UV CD spectra of ferric WT cyt c and cleft variants at pH 7 and 20 °C. (B and C) Examples of equilibrium unfolding at pH 7 for ferric WT cyt c and the R91A mutant by chemical denaturation with GdnHCl (B) and thermal denaturation (C). The solid lines represent fits to the data with the thermodynamic parameters and T_m values obtained reported in Table 1. (D) The pH dependence of the 695 nm band for WT ferric cyt c and the R91A mutant fitted to a one-proton equilibrium equation. The pK_{695} values are reported in Table 1. Protein concentrations for CD and pH titrations were 20 μM and 100 μM, respectively.

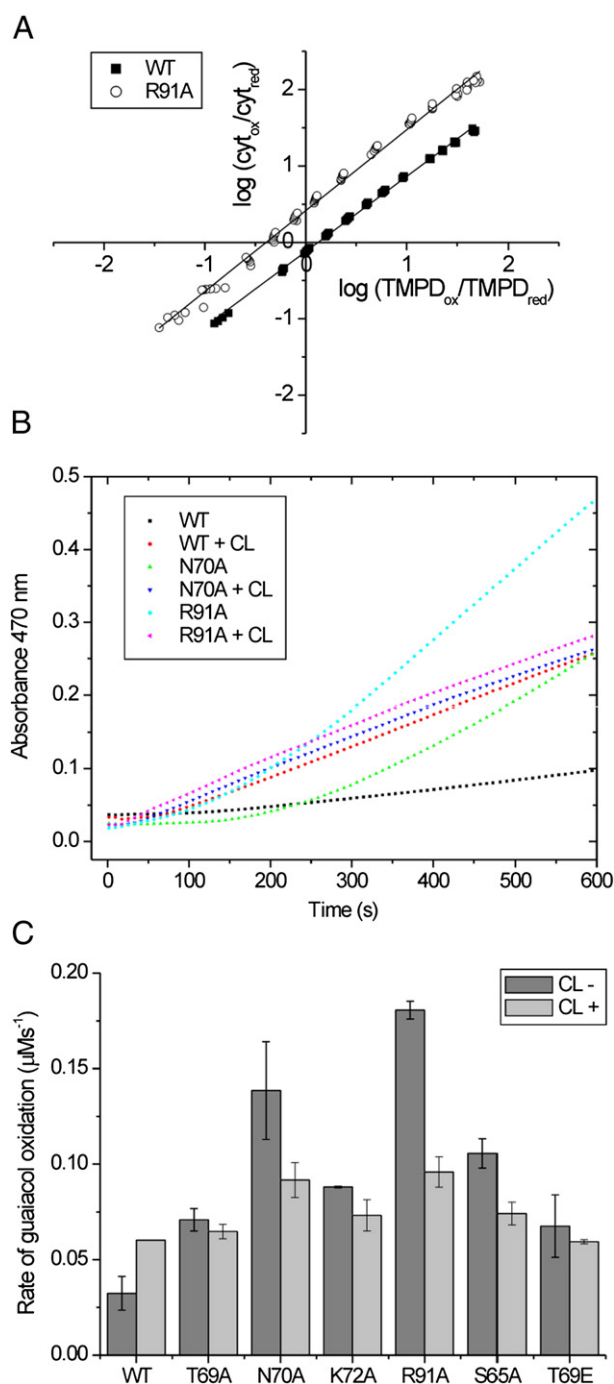**Fig. 3.** Redox potentials and peroxidase activity assays of yeast cyt *c* and cleft mutants (5 μM), pH 7.4, 22 °C. (A) The E_m of yeast cyt *c* and cleft variants was assessed spectrophotometrically using TMPD as equilibrium redox substrate and data obtained were plotted as log(TMPD$_{OX}$/TMPD$_{RED}$) versus log(cyt c_{OX}/cyt c_{RED}). The E_m for the individual proteins was determined according to the Nernst equation (see Materials and Methods). (B) Illustrative time courses for the oxidation of guaiacol in the presence of H_2O_2 for WT ferric cyt *c* and the N70A and R91A cleft mutants in the absence and presence of CL. (C) The maximal peroxidation rates of guaiacol for WT and cleft mutants in the absence and presence of 30 M equivalents of CL. The error bars are the standard deviation from measurements carried out in triplicate. Protein concentrations for peroxidase measurements were 5 μM.

conditions. All the mutants displayed a basal increase in the rate of guaiacol oxidation with R91A displaying the greatest increase, followed by N70A. In the presence of CL (30 M equivalents, *vide infra*) the initial peroxidase activity is considerably boosted for all the proteins (Fig. 3B), but this effect is primarily associated with an action of CL in abolishing a 'lag' phase seen in the absence of CL with both

the WT protein and most cleft mutants. The higher early maximal activities with CL present are thus not markedly different from those observed later, after the lag phase, in the absence of CL. The measured maximal peroxidatic turnover rates are summarized in Fig. 3C.

3.4. pH sensitivity of the ferrous cyt c/CL complex towards CO binding

The spectrum of the ferrous cyt *c*/CL complex is pH dependent. This is illustrated in Fig. 4A where the spectrum of the ferrous form of the WT protein complexed with CL is shown. Complex formation is a reversible process with full removal of CL by a combination of high salt, to disrupt electrostatic, and TritonX 100 to disrupt hydrophobic interactions, resulting in the recovery of free cyt *c* with native spectroscopic properties [18]. At low pH the spectrum is typical of a high-spin ferrous complex, indicating the possibility that the 6th coordination position is either vacant (cf ferrous myoglobin [37,38]) or a labile weak field ligand such as water is present at the 6th coordination site. On increasing the pH the protein undergoes a transition ($pK_a \sim 7.85$; inset Fig. 4A) to a low-spin ferrous form (see bands at 520 and 550 nm), consistent with a strong field ligand binding to the 6th coordination site. The pH transition also reports the capacity of the ferrous protein to bind CO; at high pH where the low-spin complex is fully populated, the protein does not bind CO, *i.e.* the intrinsic ligand cannot be displaced. We speculate that this ligand in the ferrous complex is Met-80, the intrinsic ligand of the WT protein. It is fully removed from coordination in the CL complex at low pH (high-spin species), but structural changes accompanying the pH transition of the ferrous cyt *c*/CL complex could bring Met-80 into the coordination sphere and re-ligate at alkaline pH. Although we have no experimental evidence to prove that Met-80 is acting as the ligand, the fact that Met-80 cannot be displaced by CO, characteristic of ferrous WT cyt *c*, and is unlike the behavior of *c*-type cytochromes where the sixth ligand is a Lys [26,27] gives us some leeway for speculation. The CL complex of the ferrous R91A mutant, in contrast, retains the capacity to bind CO fully at all pH values studied. At low pH in the absence of CO its spectrum indicates a 5C or 6C (with water bound) high-spin species and the high pH spectrum is consistent with that of a 6C low-spin form with a strong field ligand (Figure S1). However, the ability to bind CO at high pH suggests that unlike the WT and the other cleft mutants the pH structural change associated with the high to low-spin transition in the R91A mutant is sufficiently perturbed compared to WT so that Met-80 cannot return to the coordination sphere and instead another strong field ligand binds that can subsequently be displaced by CO.

3.5. CL and CO binding to WT ferrous cyt c and variants

The extent to which the WT and various mutants of the ferrous CL complex are able to bind CO at pH 7.4 is shown in Fig. 4B. Here we depict the normalized absorbance change on CO binding as a function of [CL]. The trend displayed by the proteins (for all expect R91A) is consistent with data that we have previously reported [18], namely that to obtain the full effect of CL requires ~25 CL molecules. This 'apparent' stoichiometry we have interpreted earlier [18], as cyt *c* binding to the membrane fragments composed of CL with each cyt *c* bound occluding ~25 CL molecules from other cyt *c* molecules and is consistent with another report using CL doped liposomes [21]. The magnitude of absorbance change on adding CO at full CL 'saturation' reflects the extent to which Met-80 is displaced from the ferrous form by CL at pH 7.4. Thus the R91A mutant, that does not have Met-80 coordinated in the presence of CL, binds CO fully, while the WT displays 70–80% CO binding, because at pH 7.4, 20–30% of the protein retains Met-80 bound at this pH as shown in Fig. 4A. For the other mutants differing amounts of CO are bound at pH 7.4, reflecting the sensitivity of the introduced mutation to the pK_a of the ferrous CL complex. The data in Fig. 4B is also shown in another way in the inset, where the data is normalized
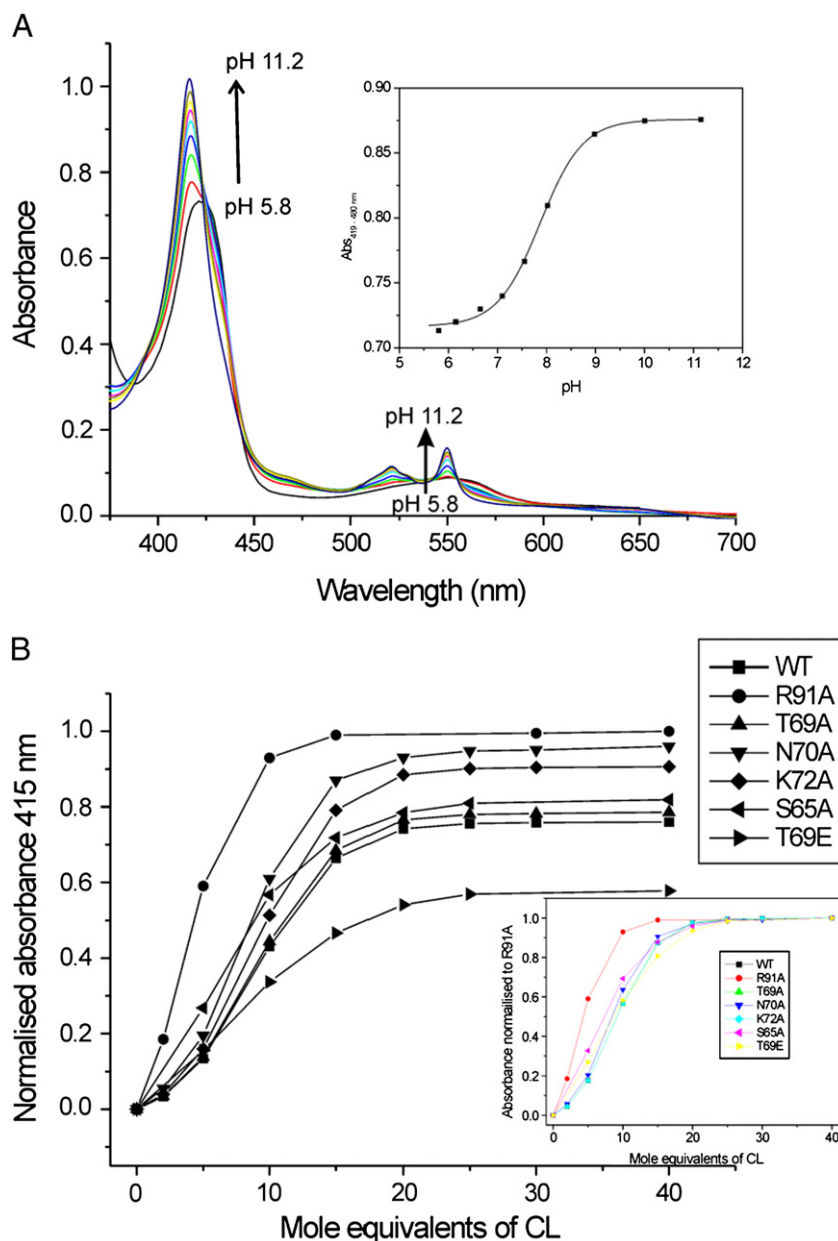
Fig. 4. (A) Changes in the visible region of the WT yeast ferrous cyt *c*/CL complex (CL in 30-fold excess) as a function of pH. The change in spin-state transition of the ferrous heme in the CL complex from high-spin at low pH to low-spin at high pH (inset) was monitored at 419 nm and fitted to a one-proton equilibrium to give a pK_{app} of 7.85. (B) Titrations of CL and CO to WT yeast ferrous cyt *c* and cleft mutants. The ΔAbs_{415nm} for the CO adduct of the ferrous proteins are plotted against molar concentration of CL. ΔAbs_{415nm} is normalized between 0 and 1, with 0 corresponding to no CO bound (no CL) and 1 to the 100% CO adduct and CL bound. The fraction of protein not converted to the CO-bound form was ascertained from the fraction of the 550 nm band remaining. Inset portrays data in B normalized to the R91A mutant. Protein concentrations used for these experiments ranged between 5 and 10 µM.

to the final end-point, with the R91A mutant being taken as unity. It is evident that the majority of the mutants behave in a fashion similar to the WT protein. In fact the transitions to plateau for WT, T69A, T69E and N70A are largely overlapping (inset Fig. 4B). The major exception is again the R91A mutant, which appears more susceptible to CL binding and to a lesser degree this is true for the S65A mutant. The R91 and S65 side-chains participate in a polar interaction with one another and in combination likely influence the stability of the cleft (Fig. 1B).

A reverse titration was carried out with the R91A mutant where ferric cyt *c* was titrated into CL to a final stoichiometry of 1:30 cyt *c*/CL. After each addition a sample was removed and the CO binding capacity of the ferrous form assessed and compared with that described above. No appreciable difference was observed in either

the shape or end-point of the curve when compared to the titration of the same mutant as shown in Fig. 4B.

3.6. Kinetics of CO binding to the ferrous cyt c/CL complex

In order to probe access to the heme-iron in the ferrous CL complex, stopped-flow and laser photolysis experiments were undertaken to follow CO binding. The two types of experiments gave essentially identical spectral properties and showed complex time courses for such binding. Laser photolysis permitted a more accurate determination of the rate of CO binding than obtained by the flow method as the pseudo-first order rates are large. Fig. 5 shows kinetic difference spectra taken at defined times after photolysis of the WT cyt *c*/CL CO complex, using the spectrum of the fully CO-bound form as the
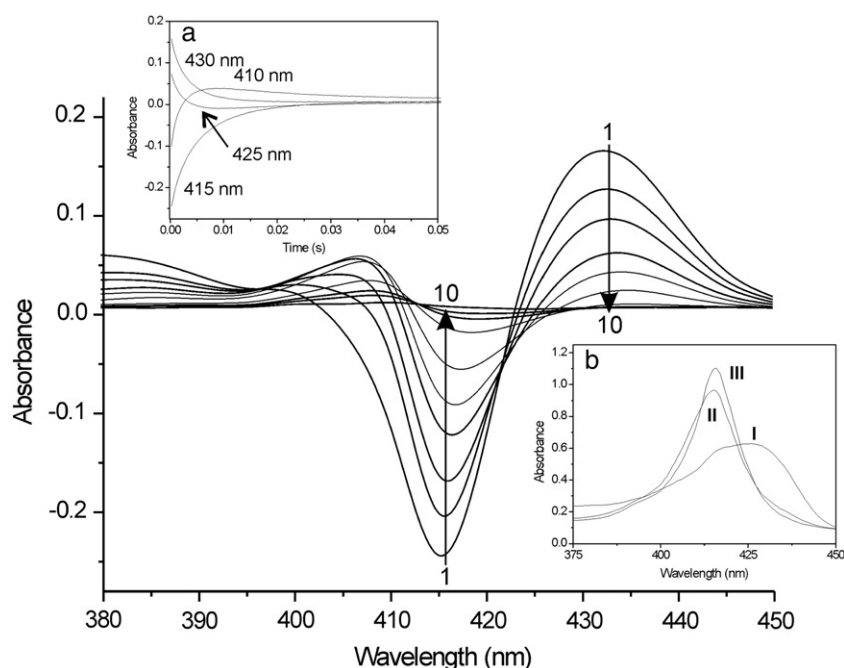
Fig. 5. Time resolved spectra of the CO adduct of the WT yeast ferrous cyt c/CL complex following laser flash photolysis at 22 °C, pH 7.4. Spectra 1–10 show CO recombination (1 = 100% CO dissociated, and 10 = 100% CO recombined) at time intervals of 0.2, 1, 2, 4, 6, 10, 20, 30, 40 and 100 ms. Time courses at different wavelengths for CO recombination are shown in inset a. Shown in inset b are spectra I and II that correspond to the 5C and 6C forms, respectively, generated from global analysis of the difference spectra and spectrum III the static CO form of the CL complex. Protein concentrations used ranged between 3 and 7 μM.

baseline. The final overall difference spectrum (taken between $t = 0$ and $t = 100$ ms) is identical to the static difference spectrum for CO binding. The lack of isosbestic points indicates the presence of more than two spectral species. This is also clear from the illustrative time courses in inset a of Fig. 5 where at some wavelengths (e.g., 410 nm) the two kinetic phases proceed in opposite directions. The spectral contributions of the two phases may be separated (global analysis (Pro K)) and added to the baseline (the CO adduct spectrum) to generate the absolute spectra of the species giving rise to the two phases. These are given in inset b of Fig. 5 normalized to provide the spectral magnitudes expected if each were the sole species present. Spectrum I is that of the fast phase previously identified as penta-coordinate (5C) cyt c [26,27]. The slower phase has the spectrum given in Fig. 5 inset b (II) and is typical of hexa coordinate (6C) low-spin cyt c. The rate constants for the two phases were measured as a function of CO concentration and the results for the R91A mutant that yields the same spectral components and overall spectra, as seen in Fig. 5, are shown in Fig. 6. Table 2 reports the rate constants obtained for the other cleft mutants and WT cyt c. The linear dependence of the pseudo-first order rate constant for the fast phase is consistent with CO binding to a 5C heme-iron. The second order rate constant is $6.4 \times 10^6 \, M^{-1} \, s^{-1}$, in agreement with that reported earlier [18] and greater than that for myoglobin and M80X mutants of yeast ferrous cyt c [27]. These results indicate unimpeded access to the 5C heme-iron from the exterior bulk phase. Fig. 6 also shows that the rate constant reaches a CO concentration independent plateau of ~130 s^{-1} at high CO levels.

4. Discussion

The discovery of a pro-apoptotic protein:lipid complex, namely cyt c/CL, has triggered a renaissance of interest in the functional properties of lipids and their influence on soluble proteins. Lipid interactions involving cyt c [6] have been known prior to the link with apoptosis and led to a number of seminal works leading up to the proposal of the extended-lipid anchorage model [15,17]. This model has found favor in interpreting the sequence of events that turns cyt
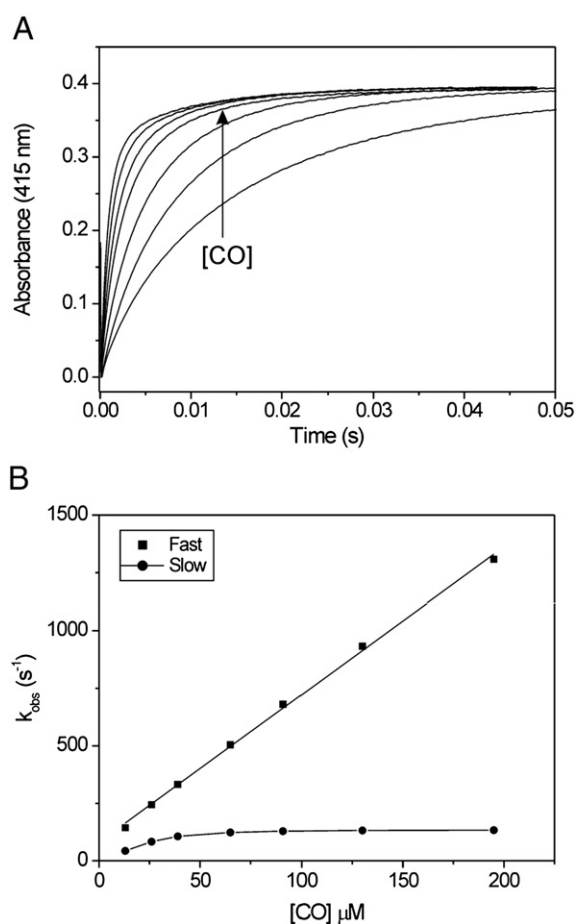

Fig. 6. Laser flash photolysis of the CO adduct of the yeast R91A ferrous cyt c/CL complex at 22 °C, pH 7.4. (A) Representative time course collected at 415 nm over a range of [CO] from 13 to 195 μM. (B) Plots of k_{obs} (s^{-1}) versus [CO] for the fast and slow phases of CO recombination. Protein concentrations used ranged between 3 and 7 μM.

Table 2
Summary of the CO laser flash photolysis kinetics of the WT yeast ferrous cyt c/CL complex and mutants. The first order rate constant (k_{obs} s^{-1}) of CO recombination following photolysis were obtained by fitting each rate trace to a double exponential fit (Fig. 6A) to give a fast and slow CO recombination rate, with the relative amplitudes of absorbance at 415 nm for each normalized to 1 (i.e., Abs$_{415 \ nm}$ (fast phase) + Abs$_{415 \ nm}$ (slow phase) = 1).

Protein	k_{obs} s^{-1} (fast)	k_{obs} s^{-1} (slow)	Amplitude change (fast)	Amplitude change (slow)
WT	543	129	0.69	0.31
S65A	670	166	0.70	0.30
T69A	540	140	0.62	0.48
T69E	665	185	0.69	0.31
N70A	620	140	0.69	0.31
K72A	520	140	0.63	0.37
R91A	560	129	0.70	0.30

c apoptotic, namely the penetration of an acyl chain into the hydrophobic interior of a cyt c molecule causing dissociation of the Met-80 from the heme-iron and exploiting the oxidative potential of the heme [5,8]. The present study has focused on using site-directed mutagenesis and small molecules to probe a putative surface cleft in the vicinity of the Met-80 that has been specifically reported [16,21] to be a putative site for acyl chain insertion of a CL molecule and by Oellerich et al. [39] as a binding site to phospholipid vesicles.

4.1. R91 is a key residue in tuning the functional properties of cyt c

The cleft mutants (other than R91A) prepared in this work reveal relatively minor changes in thermodynamic and thermal stabilities, and in E_m and pK_{695} values compared with the WT protein (Table 1). Removing residues acting as hydrogen bond donors and/or acceptors to weaken or disrupt the CL binding cleft does not significantly upset the functional integrity of cyt c to act as a redox protein. A previous study, focusing on the conserved N70 residue of cyt c using protein engineering by semi-synthesis to replace N70 by non-natural amino acids, also concluded that N70 does not radically affect the redox integrity or stability of cyt c [40].

In contrast the conserved R91 that sits at the top of the cleft (Fig. 1B) has a significant effect on the redox functionality of cyt c. Arg residues can play a number of roles in regulating protein functionality, ranging from partner recognition to a structural role [41]. 'Structural' Arg residues are classified as having hydrogen bond interactions between the guanidyl group and a minimum of three backbone carbonyls. The CL binding cleft in yeast (or horse) cyt c is held together by six hydrogen bonds, four of which are centered around the guanidyl group of R91 (Fig. 1B), but only two of which involve backbone carbonyls (Fig. 1B). Although R91 cannot therefore be strictly classed as structural, its role in cyt c stability and maintenance of the integrity of the cleft and stoichiometry of CL binding is clearly apparent.

The R91A mutant shows a decrease in E_m of 30 mV, making it thermodynamically less favorable to function efficiently in the mitochondrial ET chain at physiological pH of 7. The E_m reflects the relative energies of the ferric and ferrous proteins and therefore the introduction of mutations and their subsequent effect on the relative thermodynamic stabilities of the two heme oxidation states should ideally be determined before attempts at correlating effects to changes in E_m can be made. However, previous studies have reported a relationship between the Fe–S(Met) bond stability, pK_{695} values and E_m in cyts c [42–45]. We note here for the R91A mutant that the decrease in pK_{695} value correlates with the change in E_m for the mutant and in accordance with previous studies [42–45] can be interpreted as a weakening of the Fe–S(Met) bond stability causing a downward shift in E_m.

Our results contrast starkly with a previous study with horse cyt c where R91 was replaced by the non-natural leucine isomer, norleucine (Nle), using semi-synthetic methods [46]. Nle provides the

space filling function of an Arg side-chain but does not have the guanidyl group. This is in contrast to an Ala substitution, which creates a space in a well-packed environment that might lead to increased accessibility of the interior or distortion of local structure. Nevertheless, the replacement of Arg with Nle abolishes the intricate hydrogen bond network formed around the guanidyl group of the Arg, which we propose is essential in maintaining the stability of the ferric protein and the CL binding cleft. However, the R91Nle protein showed no change in physicochemical properties, including the pK_{695} [46], compared with the WT protein and this suggests that maintaining the packing at the top of the cleft can compensate for the loss of side-chain polar interactions. Furthermore, the binding of the R91Nle protein to liposomes was indistinguishable from that of the WT [15,46,47], but it was noted that the R91Nle protein lost the ability to rupture liposome bilayers [15,46,47]. Finally, the conserved R91 residue has also been suggested to play a prominent role in a high affinity interaction with ATP [48–51] with binding compromised in the R91Nle protein [48].

4.2. The mechanism of peroxidase activity of cyt c in the absence or presence of CL is poorly understood

In its complex with CL cyt c causes peroxidation of the bound CL and so dissociation of the complex. In the absence of CL cyt c also displays peroxidatic activity and has been used to monitor changes in the accessibility of the heme group using hydrogen peroxide as an example of a small reacting molecule. CL binding increases the initial peroxidatic activity of the ferric protein under conditions in which the overall reaction is dependent on peroxide concentration [25]. The rate of peroxide attack hence represents a measure of heme accessibility and perhaps the occurrence of significant structural changes. However, whilst this may be true, we do not have a full analysis of this behavior. For example, the final rates after the initial lag phase are sometimes lower in the presence of CL (Fig. 3B and C). CL markedly shortens the lag phases but may stabilize the heme pocket in an intermediate state with a reactivity towards peroxide between the slower and the faster configurations. Although several hydrogen donors have been used, including pinacyanol [52,53], guaiacol [25,54] and ascorbate [55], we currently have no complete mechanistic model. The reported CL-induced increases in peroxidase function may reflect observations only during the very earliest stages in peroxidatic turnover (cf. Fig. 3B). Under our experimental conditions the maximal peroxidatic turnover for yeast cyt c in the presence of CL is not markedly different from the turnover achieved after the lag phase in the absence of CL, both for WT protein and for most of the cleft mutants.

The peroxidase measurements nevertheless reveal that in the absence of CL the R91A variant has the most pronounced increase in activity compared to the WT protein and to the other cleft mutants (Fig. 3C). This suggests that the population of a 5C minor form of the protein in equilibrium with the native 6C form under native conditions is significantly more populated [54,56]. The significant decrease in pK_{695} value for the R91A mutant suggests a destabilized protein interior that makes Met-80 displacement more favorable at pH 7 and supports the interpretation of a more populated 5C peroxidase active form of this mutant.

4.3. The cleft mutants perturb the relative populations of high- and low-spin heme in the ferrous cyt c/CL complex

In the ferrous cyt c/CL complex the WT and cleft mutants display varying degrees of maximal CO binding under the experimental conditions employed (Fig. 4B). This behavior may be adequately explained by the data obtained from the pH titrations, which indicate at pH 7.4 different spin-states of the heme-iron in the ferrous/CL complex are present leading to mixed populations of 5C and 6C heme

species. As is seen from Fig. 4B the WT protein along with the T69A and S65A cleft mutants are able to maximally bind 70–80% CO at pH 7.4 indicating that 20–30% of the ferrous protein in the complex is unable to bind CO due to the presence of a strong field ligand to the heme. On the basis that CO cannot displace the ligand and bind to the ferrous heme-iron at high pH, we speculate that this ligand is the native Met-80, which is well known to have a high affinity for the neutral ferrous heme-iron under native conditions [57]. Therefore, in the flash photolysis experiments also carried out at pH 7.4, the 6C protein that is low spin and not CO bound does not participate in the experiment. We note that a recent resonance Raman study detected a 6C species at alkaline pH in the ferric cyt *c*/CL complex [24]. The sixth ligand was assigned as a Lys, which is also the case at alkaline pH in the absence of CL [58]. For the ferrous protein the heme-iron has a significantly higher affinity for a Met over a Lys residue in the absence of CL. Our data would also suggest that this appears to be the case in complex with CL. Thus despite structural distortions induced upon insertion of an acyl chain into the hydrophobic interior, it would appear that cyt *c* intercalated with CL is not fully unfolded but can exist in a relatively compact state with Met-80 and an 'alkaline' transition Lys, possibly K79, which is not involved in binding to the phospholipid bilayer, in close proximity to the heme-iron. This view is further supported by our peroxidase measurements, which in the presence of CL do not produce activity akin to a fully unfolded cyt *c* [54,56].

Three other cleft mutants bind CO to differing extents at pH 7.4. The N70A and K72A mutants have a slightly higher CO binding capacity to WT whereas for the T69E mutant CO binding is significantly reduced. In horse heart and human cyt *c* a Glu is found at sequence position 69 and at pH 7.4 both ferrous forms can bind ≥90% CO when complexed with CL [21] (unpublished results). Introduction into yeast cyt *c* of a Glu at position 69 does not increase the capacity of the ferrous protein to bind CO when complexed to CL but rather suppresses CO binding due to an almost equal distribution of 5C and 6C species at physiological pH. Furthermore the additional negative charge does not affect the CL binding stoichiometry.

At pH 7.4 the ferrous R91A/CL complex exists in forms that can readily bind CO to a 100% extent. Strikingly, at higher pH values when a 6C form is present in all mutants (including R91A) and the WT protein, the R91A mutant still retains the ability to bind CO. This suggests that R91A has a ligand other than Met-80 bound at high pH, which CO can readily displace. As indicated structurally in Fig. 1B and experimentally in Table 1 the loss of R91 alters significantly the stability of the overall ferric fold and the lower pK_{695} value is suggestive of a destabilized heme pocket. It is conceivable therefore that this will also be the case for the ferrous form and pH structural changes associated with the high- to low-spin transition are more extensive in the R91A mutant complex such that Met-80, or another equally favored intrinsic ligand that is not displaced by CO, is not in close proximity to enable re-binding to the ferrous heme-iron. Instead a possible ligand could be a Lys residue, although less favored over Met in the ferrous state, it can be readily displaced by CO. Therefore R91 is not only essential in maintaining the stability and redox integrity of cyt *c* functioning in the electron transport chain but is also important for maintaining structural stability in the pro-apoptotic CL complex whereby its absence leads to a 6C form of the protein that is susceptible to CO binding over a broad pH range.

4.4. R91A changes the stoichiometry of CL binding

We have previously reported a 1:25 cyt *c*:CL stoichiometry [18]. This model assumes CL being present not as individual molecules but as fragments of membrane leaflets and is further supported by the fact that liposomes containing CL are able to effect the structural changes with the same apparent stoichiometry of CL to cyt *c* [17], [21]. We also note a recent time-resolved FRET study, which provides
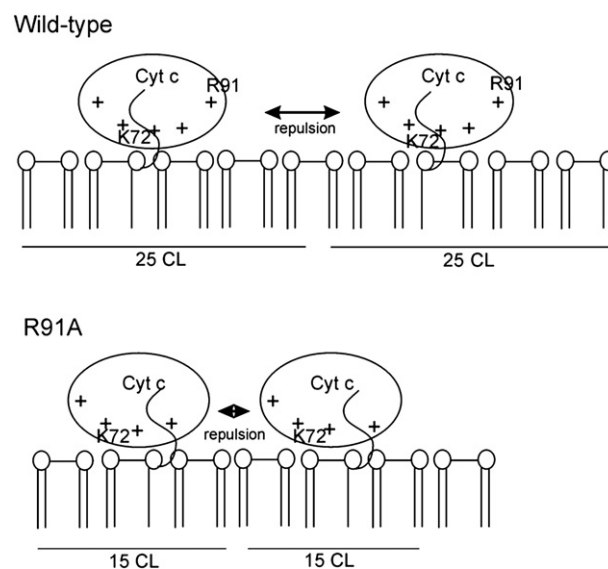

Fig. 7. A model to illustrate the stoichiometry of CL binding to cyt *c* under the experimental conditions employed in this work (i.e., in vitro). Assembly of the positively charged cyt *c* onto the negatively charged bisphosphoglycerol head groups of CL is strongly electrostatically driven. Once bound a cyt *c* molecule repels other cyt *c* molecules resulting in ~25 CL molecules covered. In this way an ordered assembly on the lipid bilayer is maintained. For the R91A mutant the electrostatic repulsion between bound cyt *c* molecules is weakened allowing a closer approach between cyt *c* molecules resulting in a stoichiometry of ~15 CL molecules.

strong evidence to suggest that a heterogeneous mixture of CL-bound cyt *c* is present ranging from compact to extended cyt *c* structures [59]. The inference from FRET measurements of the latter is a clear indication for the possibility of extensive surface coverage of the liposome by cyt *c* consistent with the cyt *c*:CL stoichiometry reported [17,18,21]. The cleft mutants, with the exception of R91A, do not perturb this CL stoichiometry and the main structural changes brought about by insertion of an acyl chain are maintained as judged from maximal CO binding. For the R91A mutant a clear shift in the stoichiometry to ~15 molecules of CL to yield maximum effect of CO binding is observed (Fig. 4B). It may be therefore, that extended conformations induced by CL in the R91A mutant are less prevalent and the removal of the positively charged Arg reduces the repulsion between compact cyt *c* molecules bound electrostatically to the CL bilayer (Fig. 7). Therefore, instead of one cyt *c* molecule covering 25–30 CL molecules ~15 molecules of CL are covered in the R91A mutant (Fig. 7). Support for this comes from previous studies, which have shown that the Lys residues 72, 73, 86 and 87 form the binding surface for anionic phospholipid-containing bilayers [22,23]. Furthermore, from studies probing ATP binding, R91 has been shown to be distinct from the lipid binding site on cyt *c* [46].

4.5. A 6C minor form populates the ferrous cyt c/CL complex

Although the fraction of the ferrous cyt *c*/CL complex that is able to bind CO depends upon the nature of the protein (i.e., WT or specific mutant) and the pH at which binding is monitored, the properties of the species that binds CO seem to be protein independent. A simple scheme can account for the kinetic data (Scheme 1). This model that applies to the WT and mutant proteins postulates that in the CO free form the main 5C species (I) is predominant and in equilibrium with a minor 6C form (II) in which an intrinsic ligand (L) is bound to the iron. Following photolysis CO rapidly binds to the 5C form ($k = 6.4 \times 10^6 \, M^{-1} \, s^{-1}$) depleting this and perturbing the equilibrium in the CO free form towards the 5C form until all the protein binds CO. At high CO concentrations, this process is rate limited by the ligand (L) dissociation rate constant, to which we thus assign a
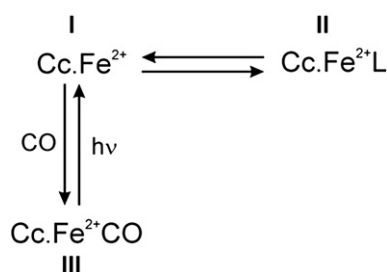
Scheme 1. A kinetic model to describe CO binding to the ferrous cyt *c*/CL complex.

value of 130 s^{-1}. This model finds support from an analysis of the relative amplitudes of the fast and slow phases depicted in Fig. 6A. On increasing CO concentration form 65 to 195 μM the proportion of the fast phase increases from 0.6 to 0.8 of the total amplitude change, while the proportion of the slow phase falls from 0.4 to 0.2 (Table S2). Such behavior is to be expected from the model shown in Scheme 1 in which following photo-dissociation the recombination reaction competes with a first order process leading to binding of an intrinsic ligand (L). Thus, the CO recombination process is more predominant at higher CO concentrations. This analysis is consistent with Scheme 1 but does not preclude a more complex model in which what we assign as a 5C high-spin species is in fact a high-spin form with a coordinated labile water molecule. At present our data cannot distinguish these possibilities.

NMR spectroscopy with M80X mutants has provided strong evidence that in the absence of external ligands the ferrous heme can coordinate the nitrogen of an amine group, most likely a Lys residue [60]. Flash photolysis studies using Met-80 modified cyt *c* and M80X mutants reveals that this ligand-iron bond to be light sensitive [26,27] and the spectra of the yeast M80X mutants with His–Lys ligation very similar to II in Fig. 5, inset b [27]. A recent magnetic circular dichroism spectroscopy study of the CL-bound states of WT ferric and ferrous cyt *c* provides strong evidence in support of a His–Lys ligation species in the ferrous cyt *c*/CL complex [11]. It is not therefore unreasonable to assume that the 6C minor form detected in our kinetic experiments (II in Scheme 1) at pH 7.4 is a ferrous form of cyt *c* with a Lys bound that is invariably replaced by CO.

4.6. Conclusions

Testing predicted CL intercalation sites on cyt *c* is not trivial. The presumed cleft we have probed in this study reveals relatively subtle differences in the biophysical and functional assays we have used, and we conclude that disruption of the cleft by Ala mutations does not appear to influence the hydrophobic interaction of CL. On the other hand this study serves to highlight that mutations considered to be benign in affecting the redox role of cyt *c*, do influence the properties of cyt *c* when complexed with CL. This is seen from the CO binding studies where the mutations appear to modulate the extent of CO binding to the ferrous heme. Of all the cleft mutants studied it can be concluded that R91 is clearly an important residue for the integrity of the native protein and also for governing the stoichiometry of the interaction with CL and the properties of the ferrous cyt *c*/CL complex especially with respect to the occupation of the sixth ligand coordination site.

Appendix A. Supplementary data

Supplementary data to this article can be found online at doi:10. 1016/j.bbabio.2012.02.010.

References

[1] Y.P. Ow, D.R. Green, Z. Hao, T.W. Mak, Cytochrome c: functions beyond respiration, Nat. Rev. Mol. Cell Biol. 9 (2008) 532–542.
[2] S.J. Riedl, G.S. Salvesen, The apoptosome: signalling platform of cell death, Nat. Rev. Mol. Cell Biol. 8 (2007) 405–413.
[3] G.W. Pettigrew, G.R. Moore, Cytochromes c. Biological aspects, Springer-Verlag, Heidelberg, Germany, 1987.
[4] X. Liu, C.N. Kim, J. Yang, R. Jemmerson, X. Wang, Induction of apoptotic program in cell-free extracts: requirement for dATP and cytochrome c, Cell 86 (1996) 147–157.
[5] V.E. Kagan, V.A. Tyurin, J. Jiang, Y.Y. Tyurina, V.B. Ritov, A.A. Amoscato, A.N. Osipov, N.A. Belikova, A.A. Kapralov, V. Kini, I.I. Vlasova, Q. Zhao, M. Zou, P. Di, D.A. Svistunenko, I.V. Kurnikov, G.G. Borisenko, Cytochrome c acts as a cardiolipin oxygenase required for release of proapoptotic factors, Nat. Chem. Biol. 1 (2005) 223–232.
[6] P. Nicholls, Cytochrome c binding to enzymes and membranes, Biochim. Biophys. Acta 346 (1974) 261–310.
[7] N.A. Belikova, Y.A. Vladimirov, A.N. Osipov, A.A. Kapralov, V.A. Tyurin, M.V. Potapovich, L.V. Basova, J. Peterson, I.V. Kurnikov, V.E. Kagan, Peroxidase activity and structural transitions of cytochrome c bound to cardiolipin-containing membranes, Biochemistry 45 (2006) 4998–5009.
[8] L.V. Basova, I.V. Kurnikov, L. Wang, V.B. Ritov, N.A. Belikova, I.I. Vlasova, A.A. Pacheco, D.E. Winnica, J. Peterson, H. Bayir, D.H. Waldeck, V.E. Kagan, Cardiolipin switch in mitochondria: shutting off the reduction of cytochrome c and turning on the peroxidase activity, Biochemistry 46 (2007) 3423–3434.
[9] A.A. Kapralov, I.V. Kurnikov, I.I. Vlasova, N.A. Belikova, V.A. Tyurin, L.V. Basova, Q. Zhao, Y.Y. Tyurina, J. Jiang, H. Bayir, Y.A. Vladimirov, V.E. Kagan, The hierarchy of structural transitions induced in cytochrome c by anionic phospholipids determines its peroxidase activation and selective peroxidation during apoptosis in cells, Biochemistry 46 (2007) 14232–14244.
[10] N.A. Belikova, Y.Y. Tyurina, G. Borisenko, V. Tyurin, A.K. Samhan Arias, N. Yanamala, P.G. Furtmuller, J. Klein-Seetharaman, C. Obinger, V.E. Kagan, Heterolytic reduction of fatty acid hydroperoxides by cytochrome c/cardiolipin complexes: antioxidant function in mitochondria, J. Am. Chem. Soc. 131 (2009) 11288–11289.
[11] J.M. Bradley, G. Silkstone, M.T. Wilson, M.R. Cheesman, J.N. Butt, Probing a complex of cytochrome C and cardiolipin by magnetic circular dichroism spectroscopy: implications for the initial events in apoptosis, J. Am. Chem. Soc. 133 (2011) 19676–19679.
[12] V. Borutaite, G.C. Brown, Mitochondrial regulation of caspase activation by cytochrome oxidase and tetramethylphenylenediamine via cytosolic cytochrome c redox state, J. Biol. Chem. 282 (2007) 31124–31130.
[13] P.K. Kinnunen, A. Koiv, J.Y. Lehtonen, M. Rytomaa, P. Mustonen, Lipid dynamics and peripheral interactions of proteins with membrane surfaces, Chem. Phys. Lipids 73 (1994) 181–207.
[14] P.K. Kinnunen, Fusion of lipid bilayers: a model involving mechanistic connection to HII phase forming lipids, Chem. Phys. Lipids 63 (1992) 251–258.
[15] M. Rytomaa, P.K. Kinnunen, Reversibility of the binding of cytochrome c to liposomes. Implications for lipid-protein interactions, J. Biol. Chem. 270 (1995) 3197–3202.
[16] J.M. Stewart, J.A. Blakely, M.D. Johnson, The interaction of ferrocytochrome c with long-chain fatty acids and their CoA and carnitine esters, Biochem. Cell Biol. 78 (2000) 675–681.
[17] E.K. Tuominen, C.J. Wallace, P.K. Kinnunen, Phospholipid-cytochrome c interaction: evidence for the extended lipid anchorage, J. Biol. Chem. 277 (2002) 8822–8826.
[18] S.M. Kapetanaki, G. Silkstone, I. Husu, U. Liebl, M.T. Wilson, M.H. Vos, Interaction of carbon monoxide with the apoptosis-inducing cytochrome c-cardiolipin complex, Biochemistry 48 (2009) 1613–1619.
[19] M. Abe, R. Niibayashi, S. Koubori, I. Moriyama, H. Miyoshi, Molecular mechanisms for the induction of peroxidase activity of the cytochrome c-cardiolipin complex, Biochemistry 50 (2011) 8383–8391.
[20] P.J. Spooner, A. Watts, Reversible unfolding of cytochrome c upon interaction with cardiolipin bilayers. 1. Evidence from deuterium NMR measurements, Biochemistry 30 (1991) 3871–3879.
[21] E. Kalanxhi, C.J. Wallace, Cytochrome c impaled: investigation of the extended lipid anchorage of a soluble protein to mitochondrial membrane models, Biochem. J. 407 (2007) 179–187.
[22] C. Kawai, F.M. Prado, G.L. Nunes, P. Di Mascio, A.M. Carmona-Ribeiro, I.L. Nantes, pH-Dependent interaction of cytochrome c with mitochondrial mimetic membranes: the role of an array of positively charged amino acids, J. Biol. Chem. 280 (2005) 34709–34717.
[23] A. Kostrzewa, T. Pali, W. Froncisz, D. Marsh, Membrane location of spin-labeled cytochrome c determined by paramagnetic relaxation agents, Biochemistry 39 (2000) 6066–6074.
[24] F. Sinibaldi, B.D. Howes, M.C. Piro, F. Polticelli, C. Bombelli, T. Ferri, M. Coletta, G. Smulevich, R. Santucci, Extended cardiolipin anchorage to cytochrome c: a model for protein-mitochondrial membrane binding, J. Biol. Inorg. Chem. 15 (2010) 689–700.

[25] F. Sinibaldi, L. Fiorucci, A. Patriarca, R. Lauceri, T. Ferri, M. Coletta, R. Santucci, Insights into cytochrome c-cardiolipin interaction. Role played by ionic strength, Biochemistry 47 (2008) 6928–6935.

[26] G. Silkstone, A. Jasaitis, M.H. Vos, M.T. Wilson, Geminate carbon monoxide rebinding to a c-type haem, Dalton Trans. (2005) 3489–3494.

[27] G. Silkstone, A. Jasaitis, M.T. Wilson, M.H. Vos, Ligand dynamics in an electron transfer protein. Picosecond geminate recombination of carbon monoxide to heme in mutant forms of cytochrome c, J. Biol. Chem. 282 (2007) 1638–1649.

[28] W.B. Pollock, F.I. Rosell, M.B. Twitchett, M.E. Dumont, A.G. Mauk, Bacterial expression of a mitochondrial cytochrome c. Trimethylation of lys72 in yeast iso-1-cytochrome c and the alkaline conformational transition, Biochemistry 37 (1998) 6124–6131.

[29] J. Braman, C. Papworth, A. Greener, Site-directed mutagenesis using double-stranded plasmid DNA templates, Methods Mol. Biol. 57 (1996) 31–44.

[30] M.M. Santoro, D.W. Bolen, A test of the linear extrapolation of unfolding free energy changes over an extended denaturant concentration range, Biochemistry 31 (1992) 4901–4907.

[31] T. Hosoya, J. Biochem. 48 (1960) 178–189.

[32] R.J. DeLange, A.N. Glazer, E.L. Smith, Identification and location of episilon-N-trimethyllysine in yeast cytochromes c, J. Biol. Chem. 245 (1970) 3325–3327.

[33] G. Battistuzzi, M. Borsari, F. De Rienzo, G. Di Rocco, A. Ranieri, M. Sola, Free energy of transition for the individual alkaline conformers of yeast iso-1-cytochrome c, Biochemistry 46 (2007) 1694–1702.

[34] C. Greenwood, G. Palmer, Evidence for the existence of two functionally distinct forms cytochrome c manomer at alkaline pH, J. Biol. Chem. 240 (1965) 3660–3663.

[35] X.L. Hong, D.W. Dixon, NMR study of the alkaline isomerization of ferricyto-chrome c, FEBS Lett. 246 (1989) 105–108.

[36] G.R. Moore, Protein Electron Transfer, 1996, pp. 189–216.

[37] G.S. Kachalova, A.N. Popov, H.D. Bartunik, A steric mechanism for inhibition of CO binding to heme proteins, Science 284 (1999) 473–476.

[38] F. Yang, G.N. Phillips Jr., Crystal structures of CO-, deoxy- and met-myoglobins at various pH values, J. Mol. Biol. 256 (1996) 762–774.

[39] S. Oellerich, S. Lecomte, M. Paternostre, T. Heimburg, P. Hildebrandt, Peripheral and integral binding of cytochrome c to phospholipids vesicles, J. Phys. Chem. B 108 (2004) 3871–3878.

[40] C.J. Wallace, I. Clark-Lewis, A rationale for the absolute conservation of Asn70 and Pro71 in mitochondrial cytochromes c suggested by protein engineering, Biochemistry 36 (1997) 14733–14740.

[41] C.L. Borders Jr., J.A. Broadwater, P.A. Bekeny, J.E. Salmon, A.S. Lee, A.M. Eldridge, V.B. Pett, A structural role for arginine in proteins: multiple hydrogen bonds to backbone carbonyl oxygens, Protein Sci. 3 (1994) 541–548.

[42] Y. Yamamoto, N. Terui, N. Tachiiri, K. Minakawa, H. Matsuo, T. Kameda, J. Hasegawa, Y. Sambongi, S. Uchiyama, Y. Kobayashi, Y. Igarashi, Influence of amino acid side chain packing on Fe-methionine coordination in thermostable cytochrome C, J. Am. Chem. Soc. 124 (2002) 11574–11575.

[43] N. Terui, N. Tachiiri, H. Matsuo, J. Hasegawa, S. Uchiyama, Y. Kobayashi, Y. Igarashi, Y. Sambongi, Y. Yamamoto, Relationship between redox function and protein stability of cytochromes c, J. Am. Chem. Soc. 125 (2003) 13650–13651.

[44] S.J. Takayama, S. Mikami, N. Terui, H. Mita, J. Hasegawa, Y. Sambongi, Y. Yamamoto, Control of the redox potential of Pseudomonas aeruginosa cytochrome c551 through the Fe-Met coordination bond strength and pKa of a buried heme propionic acid side chain, Biochemistry 44 (2005) 5488–5494.

[45] B.S. Rajagopal, M.T. Wilson, D.S. Bendall, C.J. Howe, J.A. Worrall, Structural and kinetic studies of imidazole binding to two members of the cytochrome c (6) family reveal an important role for a conserved heme pocket residue, J. Biol. Inorg. Chem. 16 (2011) 577–588.

[46] E.K. Tuominen, K. Zhu, C.J. Wallace, I. Clark-Lewis, D.B. Craig, M. Rytomaa, P.K. Kinnunen, ATP induces a conformational change in lipid-bound cytochrome c, J. Biol. Chem. 276 (2001) 19356–19362.

[47] E.K. Tuominen, C.J. Wallace, P.K. Kinnunen, The invariant ARG91 is required for the rupture of liposomes by cytochrome C, Biochem. Biophys. Res. Commun. 238 (1997) 140–142.

[48] D.B. Craig, C.J. Wallace, ATP binding to cytochrome c diminishes electron flow in the mitochondrial respiratory pathway, Protein Sci. 2 (1993) 966–976.

[49] D.B. McIntosh, J.C. Parrish, C.J. Wallace, Definition of a nucleotide binding site on cytochrome c by photoaffinity labeling, J. Biol. Chem. 271 (1996) 18379–18386.

[50] D.B. Craig, C.J. Wallace, Studies of 8-azido-ATP adducts reveal two mechanisms by which ATP binding to cytochrome c could inhibit respiration, Biochemistry 34 (1995) 2686–2693.

[51] A. Patriarca, T. Eliseo, F. Sinibaldi, M.C. Piro, M. Melis, M. Paci, D.O. Cicero, F. Polticelli, R. Santucci, L. Fiorucci, ATP acts as a regulatory effector in modulating structural transitions of cytochrome c: implications for apoptotic activity, Biochemistry 48 (2009) 3279–3287.

[52] B. Valderrama, H. Garcia-Arellano, S. Giansanti, M.C. Baratto, R. Pogni, R. Vazquez-Duhalt, Oxidative stabilization of iso-1-cytochrome c by redox-inspired protein engineering, FASEB J. 20 (2006) 1233–1235.

[53] J.A. Villegas, A.G. Mauk, R. Vazquez-Duhalt, A cytochrome c variant resistant to heme degradation by hydrogen peroxide, Chem. Biol. 7 (2000) 237–244.

[54] R.E. Diederix, M. Ubbink, G.W. Canters, Peroxidase activity as a tool for studying the folding of c-type cytochromes, Biochemistry 41 (2002) 13067–13077.

[55] C. Bischin, F. Deac, R. Silaghi-Dumitrescu, J.A. Worrall, B.S. Rajagopal, G. Damian, C.E. Cooper, Ascorbate peroxidase activity of cytochrome c, Free. Radic. Res. 45 (2011) 439–444.

[56] J.A. Worrall, R.E. Diederix, M. Prudencio, C.E. Lowe, S. Ciofi-Baffoni, M. Ubbink, G.W. Canters, The effects of ligand exchange and mobility on the peroxidase activity of a bacterial cytochrome c upon unfolding, ChemBioChem 6 (2005) 747–758.

[57] G.R. Moore, G.W. Pettigrew, Cytochrome c: Evolutionary, Structural and Physico-chemical Aspects, Springer-Verlag, London, 1990.

[58] M. Assfalg, I. Bertini, A. Dolfi, P. Turano, A.G. Mauk, F.I. Rosell, H.B. Gray, Structural model for an alkaline form of ferricytochrome C, J. Am. Chem. Soc. 125 (2003) 2913–2922.

[59] J. Hanske, J.R. Toffey, A.M. Morenz, A.J. Bonilla, K.H. Schiavoni, E.V. Pletneva, Conformational properties of cardiolipin-bound cytochrome c, Proc. Natl. Acad. Sci. U. S. A. 109 (2012) 125–130.

[60] G. Silkstone, G. Stanway, P. Brzezinski, M.T. Wilson, Production and character-isation of Met80X mutants of yeast iso-1-cytochrome c: spectral, photochemi-cal and binding studies on the ferrous derivatives, Biophys. Chem. 98 (2002) 65–77.